Z. Phys. Chem. **217** (2003) 365–381

Quantitative Modeling of the Oscillatory Electrooxidation of Hydrogen on Pt in the Presence of Poisons

By F. Plenge[1], H. Varela[1], M. Lübke[1], and K. Krischer[1,2,*]

[1] Fritz-Haber-Institut der Max-Planck-Gesellschaft, Faradayweg 4–6, 14195 Berlin, Germany
[2] Fakultät für Physik, Technische Universität München, James-Franck-Str. 1, 85748 Garching, Germany

Dedicated to Prof. Dr. Dieter M. Kolb on the occasion of his 60th birthday

(Received August 9, 2002; accepted in revised form November 5, 2002)

Hydrogen Oxidation / Electrochemical Oscillations / Nonlinear Dynamics / Cu Underpotential Deposition

A quantitative model of oscillations observed during hydrogen oxidation on platinum in the presence of electrosorbing metal ions and specifically adsorbing anions is presented and the model predictions are compared with experiments. Mass and charge balances of all reactants lead in a first step to a seven variable model which is governed by reaction steps that have been widely studied. We demonstrate that attractive interactions between metal and halide ions on the electrode surface, which were recently reported [1], are crucial for the observed dynamics. The model parameters were almost exclusively taken out of the literature. The model is then reduced to its minimal form without losing dynamic features arriving at a four variable system. Experimental time series of three of the four variables of the model and measured bifurcation diagrams are presented. It is shown that the integrated time evolution and the calculated bifurcation diagrams of the model agree almost quantitatively with the experiment.

1. Introduction

The hydrogen oxidation reaction (HOR) on platinum electrodes is one of the most widely studied electrochemical reactions. Oscillations in this system are known to exist since 1930 [2]. Horányi was the first to show that the HOR exhibits oscillations in the presence of electrosorbing metal ions under galvanostatic conditions [3]. In a series of papers at the beginning of the 90 s some

* Corresponding author. E-mail: krischer@ph.tum.de

of us proofed the essential role anions play in the oscillation mechanism [4–6] speculated about earlier [3, 7]. Furthermore we showed that oscillations also occur under potentiostatic conditions for sufficiently high series resistance (either through the electrolyte solution, R_Ω, or due to an external resistance, R_{ext}) [6].

Taking into account the potential dependent coverages of metal and halide ions the oscillations could be modeled [4–6]. But prominent features of the oscillatory behavior could not be captured in these simulations. This calls for a more detailed description since the hydrogen oxidation on Pt in the presence of electrosorbing ions constitutes a prototype model for the study of dynamic instabilities in electrochemical systems for three reasons:

(a) The observed dynamics is very rich: Period doubling cascades, chaotic dynamics with an interior crisis and mixed-mode oscillations were reported already a decade ago [8–11]. In recent measurements of pattern formation during the HOR in the presence of Cu^{2+} and Cl^- we observed novel spatio-temporal phenomena which seem to be connected to the relaxation like form of the underlying oscillations [12, 13] that could not be reproduced by the models studied in [4–6].

(b) The mechanism that leads to oscillations during the HOR is well understood and is made up of reaction steps that are independently studied. Recent investigations by Marković and Ross provided new insight into the interactions between the involved species [1, 14, 15] that were not accounted for in earlier models. We show in this paper that these interactions are essential for realistic modeling of the HOR.

(c) The oscillatory dynamics of four quantities including three of the essential variables of the system are accessible experimentally and presented in this paper. This exceptional situation allows the observation of the phase relations of these variables and thus a compelling test of a proposed model.

A quantitative model of the oscillatory HOR is thus both needed and feasible and the model can then be solidly verified with the experimental data.

Electrocatalytic reactions involve the adsorption of reaction intermediates or an educt on the working electrode surface. This causes a strong dependence of the reaction rate on the composition of the electrolyte since species dissolved in the electrolyte may also adsorb on the electrode surface. These adsorbates often accelerate or inhibit the reaction under consideration. The essential ingredient of the model presented in [4–6] to rationalize the occurrence of oscillations during H_2 oxidation in the presence of electrosorbing ions is that both dissolved species adsorb at the electrode surface and block the occupied surface sites for the HOR. The third variable necessary to describe the oscillations is the double layer potential, ϕ_{DL}, measuring the voltage drop across the interface between the working electrode and the electrolyte solution. The adsorption of metal ions occurs at low potentials and the electrode is practically free of metal ions above a certain ϕ_{DL}. The halide ions behave in just the opposite way. For the rest of the paper underpotential deposition of Cu^{2+}

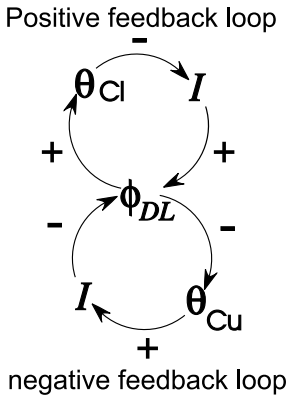

Fig. 1. Schematic plot of activator (positive feedback) and inhibitor (negative feedback) loops.

(occurring at low potentials) and specific adsorption of Cl^- (favored at more positive potentials) are taken to be the metal respectively halide ions if not stated otherwise.

The opposite potential dependence of the adsorption of Cu^{2+} and Cl^- is the crucial mechanistic feature causing the oscillatory instability (the following applies to potentiostatic control which is also used in the rest of the paper, but the general mechanism is the same for the galvanostatic case and the presented model applies also under galvanostatic conditions). Consider a situation where the Pt-surface is almost free of adsorbates, *i.e.* the oxidation current is high and ϕ_{DL} is low. At low ϕ_{DL} Cu^{2+} ions adsorb slowly, which causes the current to decrease, and, thus, for a non-negligible cell resistance, ϕ_{DL} increases. At more positive values of ϕ_{DL} Cu starts eventually to desorb and Cl^- ions to adsorb. As illustrated in Fig. 1, the increase in chloride coverage with increasing potential initiates an autocatalytic process (positive feedback loop): An increase in the Cl^- coverage, θ_{Cl}, leads to a smaller current density, a smaller current density to a larger value of ϕ_{DL} and thus to a further increase in θ_{Cl}. The decrease in Cu coverage with increasing potential, on the other hand, causes an increase in current density which inhibits the further growth of ϕ_{DL}. Thus, it generates a negative feedback loop. Owing to the faster adsorption/desorption rates of Cl as compared to Cu, the characteristic time of the positive feedback loop is shorter than the one of the negative feedback loop. This causes the above mentioned initial increase in ϕ_{DL} due to Cu adsorption to be enhanced owing to Cl^- adsorption. Only at these larger values of ϕ_{DL} will Cu desorption be sufficiently fast to cause a decrease in ϕ_{DL} again. This decrease of ϕ_{DL} now prompts a decrease in Cl^- coverage, initiating again the autocatalytic process, this time to smaller values of ϕ_{DL}. In this way, the system arrives back at a state where the surface is almost copper and chloride free, and the cycle starts anew.

The model presented in [4] included the two coverages and the double layer potential, but neglected the dependence of the hydrogen current on ϕ_{DL}.[1] It was able to reproduce the general oscillatory behavior, *i.e.* it showed qualitative agreement of bifurcation diagrams with experiment. The main features not captured in this model are the form of the oscillations and the drop of the double layer potential to values near the equilibrium potential of the hydrogen oxidation/evolution reaction. A third important feature not described by the above model is the apparently hard onset of the oscillations at low voltages observed in the experiment during an anodic scan of the applied voltage (*cf.* Fig. 3(a) and [12, 13]). And finally, the phase relations given by the model in [4] were only matching the experimental ones close to the Hopf bifurcation and at high conductivity.

In the next section we will show that, when including up to seven variables in the dynamics, almost quantitative agreement with the experiments can be reached. It is important to note that the model predictions are obtained using a large number of physical constants which are almost exclusively taken out of the literature and are thus obtained independently and not fitted to the experiment (see Table 1). The model will then be reduced to the minimal model still capturing all features of the dynamics observed in experiment. The results obtained are compared in detail with experiments using Cl^- or Br^- as halide ion. The experimental techniques and computational methods used are given in the Appendix.

2. Model

The starting point for the subsequent modeling are the chemical processes which will be taken into account:

$$\mathrm{Cu^{2+} + 2e^- + *} \underset{k^{\mathrm{d}}_{\mathrm{Cu}}}{\overset{k^{\mathrm{a}}_{\mathrm{Cu}}}{\rightleftharpoons}} \mathrm{Cu_{ad}} \tag{1}$$

$$\mathrm{Cl^- + *} \underset{k^{\mathrm{d}}_{\mathrm{Cl}}}{\overset{k^{\mathrm{a}}_{\mathrm{Cl}}}{\rightleftharpoons}} \mathrm{Cl^{-+\delta}_{ad} + \delta e^-} \tag{2}$$

$$\mathrm{H_2 + **} \underset{k^{\mathrm{d}}_{\mathrm{H}}}{\overset{k^{\mathrm{a}}_{\mathrm{H}}}{\rightleftharpoons}} \mathrm{2H_{ad}} \tag{3}$$

$$\mathrm{H_{ad}} \underset{k^{\mathrm{r}-}_{\mathrm{H}}}{\overset{k^{\mathrm{r}+}_{\mathrm{H}}}{\rightleftharpoons}} \mathrm{H^+ + e^-} \tag{4}$$

[1] In [5] also a model with potential dependent hydrogen current was presented, but the potential dependence was phenomenological and based on a non-langmuiric behavior of the current which was falsified by the realistic model presented here (s.b.).

('$*$' denotes a free surface site). For reactions (1–3) the species on the left hand side are considered to be in the reaction plane and the transport from the bulk to the reaction plane has also to be taken into account. We consider here the Tafel–Volmer mechanism for the HOR [16]. The variables included in the model to describe the mechanism (1–4) are the double layer potential, ϕ_{DL}, the coverage of the electrode by hydrogen, chloride and copper, θ_H[2], θ_{Cl}, θ_{Cu}, and the concentrations in the reaction plane, c_H, c_{Cl}, c_{Cu}.

The dynamics of the double layer potential is given by (a) the control condition

$$i = (U - \phi_{DL})(AR_t)^{-1} \tag{5}$$

(i is the total current density, U denotes the applied voltage, A the working electrode area and $R_t = R_{ext} + R_\Omega$ the total resistance) and (b) the local charge balance of capacitive, i_c, and reactive, i_r, current densities, $i = i_c + i_r$, where $i_c = C\dot{\phi}_{DL}$ and $i_r = i_{H_2} + i_{Cu} + i_{Cl}$. Here C denotes the capacity of the double layer per unit area and i_{H_2}, i_{Cu}, and i_{Cl} are the current densities due to hydrogen oxidation and copper and chloride adsorption/desorption, respectively. Under our experimental conditions the currents due to (partial) discharge of Cu^{2+} and Cl^- can be neglected. They contribute far less than 5% to the total current density. Thus, in the model, we take $i_r = i_{H_2}$. i_{H_2} is modeled using Butler-Volmer kinetics neglecting the hydrogen evolution reaction (HER). The change in coverages is given by the difference between adsorption and desorption velocities supplemented with 'consumptive' reaction in the case of hydrogen. H_{ad}, Cu^{2+} and Cl^- are considered to compete for the same surface sites with the exception that Cu^{2+} adsorption is not hindered by H_{ad}. Considering recent experiments by Stamenković *et al.* [1] we assume an attractive interaction between Cu^{2+} and Cl^- in the sense that anion adsorption is enhanced in the presence of copper on the electrode surface. This was not done in previous models and it turned out that it is essential for a correct description of the dynamics. We do not take any other interactions between the different species into account. The temporal changes of the concentrations of the individual species are given by the sum of adsorption, desorption and diffusion from the bulk solution to the 'reaction' plane.

The set of dynamic equations is thus

$$C\dot{\phi}_{DL} = -i_r + i \tag{6}$$

$$\frac{\delta_H}{2}\dot{c}_H = \frac{D_H}{\delta_H}\left(c_H^b - c_H\right) - \left(v_H^a - v_H^d\right) \tag{7}$$

[2] We only consider the reactive adsorbate H_{ad} (sometimes called H_{opd}) and neglect any influences on the dynamics by underpotentially adsorbed hydrogen, H_{upd}.

$$\frac{\delta_{\mathrm{Cu}}}{2}\dot{c}_{\mathrm{Cu}} = \frac{D_{\mathrm{Cu}}}{\delta_{\mathrm{Cu}}}\left(c^{\mathrm{b}}_{\mathrm{Cu}} - c_{\mathrm{Cu}}\right) - \left(v^{\mathrm{a}}_{\mathrm{Cu}} - v^{\mathrm{d}}_{\mathrm{Cu}}\right) \tag{8}$$

$$\frac{\delta_{\mathrm{Cl}}}{2}\dot{c}_{\mathrm{Cl}} = \frac{D_{\mathrm{Cl}}}{\delta_{\mathrm{Cl}}}\left(c^{\mathrm{b}}_{\mathrm{Cl}} - c_{\mathrm{Cl}}\right) - \left(v^{\mathrm{a}}_{\mathrm{Cl}} - v^{\mathrm{d}}_{\mathrm{Cl}}\right) \tag{9}$$

$$N\dot{\theta}_{\mathrm{H}} = v^{\mathrm{a}}_{\mathrm{H}} - v^{\mathrm{d}}_{\mathrm{H}} - i_{\mathrm{r}}/F \tag{10}$$

$$N\dot{\theta}_{\mathrm{Cu}} = v^{\mathrm{a}}_{\mathrm{Cu}} - v^{\mathrm{d}}_{\mathrm{Cu}} \tag{11}$$

$$N\dot{\theta}_{\mathrm{Cl}} = v^{\mathrm{a}}_{\mathrm{Cl}} - v^{\mathrm{d}}_{\mathrm{Cl}} \tag{12}$$

with

$$\begin{aligned}
v^{\mathrm{a}}_{\mathrm{H}} - v^{\mathrm{d}}_{\mathrm{H}} &= c_{\mathrm{H}} k^{\mathrm{a}}_{\mathrm{H}} \left(1 - \theta_{\mathrm{H}} - \theta_{\mathrm{Cu}} - \theta_{\mathrm{Cl}}\right)^2 - k^{\mathrm{d}}_{\mathrm{H}} \theta^2_{\mathrm{H}} \\
v^{\mathrm{a}}_{\mathrm{Cu}} - v^{\mathrm{d}}_{\mathrm{Cu}} &= k^{\mathrm{a}}_{\mathrm{Cu}} c_{\mathrm{Cu}} \left(1 - \theta_{\mathrm{Cu}} - \theta_{\mathrm{Cl}}\right) - k^{\mathrm{d}}_{\mathrm{Cu}} \theta_{\mathrm{Cu}} \\
v^{\mathrm{a}}_{\mathrm{Cl}} - v^{\mathrm{d}}_{\mathrm{Cl}} &= k^{\mathrm{a}}_{\mathrm{Cl}} c_{\mathrm{Cl}} \left(1 + \chi\theta_{\mathrm{Cu}}\right) \left(1 - \theta_{\mathrm{H}} - \theta_{\mathrm{Cu}} - \theta_{\mathrm{Cl}}\right) - k^{\mathrm{d}}_{\mathrm{Cl}} \theta_{\mathrm{Cl}} \\
i_{\mathrm{r}} &= F k^{r+}_{\mathrm{H}} \theta_{\mathrm{H}} \left(\mathrm{e}^{a_{\mathrm{H}}\phi_{\mathrm{DL}}} - 1\right)
\end{aligned}$$

and

$$\begin{aligned}
k^{\mathrm{a}}_{\mathrm{Cu/Cl}} &= k^{\mathrm{a},0}_{\mathrm{Cu/Cl}} \mathrm{e}^{-a_{\mathrm{Cu/Cl}}\left(\phi_{\mathrm{DL}} - \phi^{\mathrm{Cu/Cl},0}_{\mathrm{DL}}\right)} \\
k^{\mathrm{d}}_{\mathrm{Cu/Cl}} &= k^{\mathrm{d},0}_{\mathrm{Cu/Cl}} \mathrm{e}^{a_{\mathrm{Cu/Cl}}\left(\phi_{\mathrm{DL}} - \phi^{\mathrm{Cu/Cl},0}_{\mathrm{DL}}\right)}.
\end{aligned}$$

$c^{\mathrm{b}}_{\mathrm{Cu}}$ and $c^{\mathrm{b}}_{\mathrm{Cl}}$ denote the bulk concentrations of copper and chloride, respectively. $c^{\mathrm{b}}_{\mathrm{H}}$ is the bulk concentration of hydrogen for a saturated solution. v^{a}_{x} and v^{d}_{x} are the adsorption and desorption velocities of species x, respectively. N denotes the number of free surface sites per unit area on Pt. δ_{H}, δ_{Cu} and δ_{Cl} are the thicknesses of the diffusion layers for hydrogen, copper and chloride, respectively. The parameter values used for the computations are given in Tables 1 and 2, if not stated otherwise. The parameters given in Table 2 refer to the ring working electrode used in experiments concerned with spatially extended systems [12, 13]. For the experiments presented in this paper disk electrodes with diameters of 5 and 6 mm were used to exclude spatial effects (s.b.). The voltages are taken relative to the equilibrium potential of the HOR/HER. a_x quantifies the potential dependence of the adsorption/desorption processes which (since $\alpha_x = 0.5$ for simplicity) are determined by $a_x = \alpha_x n_x F(RT)^{-1} = (1-\alpha_x) n_x F(RT)^{-1}$ and n_x is the number of transfered electrons during the adsorption/desorption process. The enhanced Cl^- adsorption in the presence of Cu^{2+} is modeled by multiplying the adsorption term with $(1+\chi\theta_{\mathrm{Cu}})$ where χ is a dimensionless phenomenological constant measuring the strength of the interaction (*cf.* e.g. [23]). χ was adjusted to match model and experiment.

Table 1. Physical constants.

c_H^b	$= 7.14 \times 10^{-6}\,\mathrm{mol\,cm^{-3}}$ [a]	ν	$= 1.07 \times 10^{-2}\,\mathrm{cm^2\,s^{-1}}$ [15]
k_H^{r+}	$= 5 \times 10^{-6}\,\mathrm{mol\,s^{-1}\,cm^{-2}}$ [17]	k_H^a	$= 2.17 \times 10^{-2}\,\mathrm{cm\,s^{-1}}$ [18]
k_H^d	$= 1 \times 10^{-5}\,\mathrm{mol\,s^{-1}\,cm^{-2}}$ [17]	a_H	$= 19.5\,\mathrm{V^{-1}}$ [5]
N	$= 2.2 \times 10^{-9}\,\mathrm{mol\,cm^{-2}}$ [17]	$k_{Cl}^{a,0}/N$	$= 1 \times 10^4\,\mathrm{cm^3\,(mol\,s)^{-1}}$ [e]
D_{Cu}	$= 1.2 \times 10^{-5}\,\mathrm{cm^2\,s^{-1}}$ [19]	a_{Cl}	$= -3\,\mathrm{V^{-1}}$ [5]
$\phi_{DL}^{Cl,0}$	$= -0.5\,\mathrm{V}$ [b]	$k_{Cl}^{d,0}/k_{Cl}^{a,0}$	$= 1 \times 10^{-3}\,\mathrm{mol\,cm^{-3}}$ [e]
$k_{Cu}^{a,0}/N$	$= 1 \times 10^2\,\mathrm{cm^3\,(mol\,s)^{-1}}$ [c]	F	$= 9.64 \times 10^4\,\mathrm{C\,mol^{-1}}$
a_{Cu}	$= 38\,\mathrm{V^{-1}}$ [5]	$\phi_{DL}^{Cu,0}$	$= 0.5\,\mathrm{V}$ [b]
$k_{Cu}^{d,0}/k_{Cu}^{a,0}$	$= 1 \times 10^{-3}\,\mathrm{mol\,cm^{-3}}$ [e]	C	$= 2.0 \times 10^{-5}\,\mathrm{As\,V^{-1}\,cm^{-2}}$ [17]
D_H	$= 3.7 \times 10^{-5}\,\mathrm{cm^2\,s^{-1}}$ [a]	χ	$= 50$
D_{Cl}	$= D_{Cu}$ [f]	δ_{Cl}	$= \delta_{Cu}$ [f]
δ_H	$= \frac{1.61 D_H^{1/3} \nu^{1/6} w^{-1/2} (r_3^3 - r_2^3)^{1/3}}{r} = 3.76 \times 10^{-4}\,\mathrm{cm}$ [d]		
δ_{Cu}	$= \left(\frac{D_{Cu}}{D_H}\right)^{1/3} \delta_H = 2.54 \times 10^{-4}\,\mathrm{cm}$		

[a] Taken from [15] for $T = 25\,^\circ\mathrm{C}$ and a solution of 0.5 M H_2SO_4. Conway *et al.* give slightly different values [18].

[b] In [5] $\phi_{DL}^{Cl,0}$ and $\phi_{DL}^{Cu,0}$ were given as -0.6 and 0.6 respectively, but they depend on multiple parameters like crystal orientation and electrolyte composition. I.e. $\phi_{DL}^{Cl,0}$ was also reported to be more positive, e.g. in [20], and in [21, 22] $\phi_{DL}^{Cu,0}$ was reported to be more negative.

[c] Factor 10 lower than in [5]. This value agrees with the observed transient times.

[d] The thickness of the diffusion layers is calculated assuming a ring geometry with the outer and inner diameters r_3 and r_2, respectively, and a rotation rate of ω [16].

[e] No reliable data could be found in the literature, we thus take the values given in [5].

[f] This is a good approximation, but note that the dynamcis doesn't depend on these values (see Sect. 3.3).

Table 2. Typical parameter values used in our experiments.

c_{Cl}	$= 1 \times 10^{-7}\,\mathrm{mol\,cm^{-3}} = 0.1\,\mathrm{mM}$
c_{Cu}^b	$= 1 \times 10^{-9}\,\mathrm{mol\,cm^{-3}} = 1 \times 10^{-3}\,\mathrm{mM}$
R_t	$= 450\,\Omega$
A	$= 0.911\,\mathrm{cm^2}$
ω	$= 2\pi \times 20\,\mathrm{s^{-1}}$
r_3	$= 1.5\,\mathrm{cm}$
r_2	$= 1.45\,\mathrm{cm}$

3. Results

3.1 Stationary behavior

In Fig. 2(b) the stationary states of Eqs. (6–12) are shown in the intuitive (i, ϕ_{DL}) plane for three situations: a) In hydrogen saturated sulfuric acid ($c_{Cu} = c_{Cl} = 0$, solid line). b) In hydrogen saturated sulfuric acid solution containing Cl^- ($c_{Cu} = 0$, dashed line) and c) in the presence of all three species (dotted line). The stationary states are then compared to the experiment, Fig. 2(a) (ϕ_{DL} is obtained by subtracting the IR_t drop from the

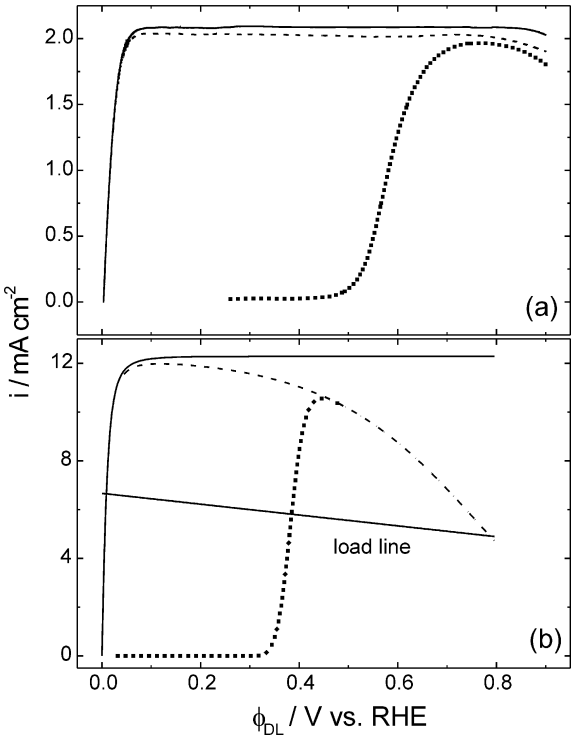

Fig. 2. (a) Stationary states in the experiments (a) and the model (b) in the presence of both poisons (dotted line), without Cu^{2+} (dashed line) and without Cl^- and Cu^{2+} (solid line) in the (i, ϕ_{DL}) plane. In the experiments ϕ_{DL} was obtained by subtracting the IR_t drop from the applied voltage U and the scan rate of $2\,mV\,s^{-1}$ yielded quasi-stationary polarization curves. In all experiments H_2 was continously bubbled through the solution. The data with Cu^{2+} were obtained using 1 mM H_2SO_4, 0.025 mM $CuSO_4$ and 1 mM Cl^- electrolyte solution thus being identical to those in Fig. 3. The two other curves were recorded with 0.1 M H_2SO_4 (for further experimental details see Appendix). In (b) the load line, Eq. (5), is also shown for $U = 3\,V$. The same concentrations were used for the computations and the other constants are given in Tables 1 and 2 except that $\phi_{DL}^{Cl,0} = -0.3\,V$.

applied voltage). For steady state conditions the capacitive current, i_c, vanishes and the HOR-current density exactly equals the total current density set by the control condition, Eq. (5), without any contributions from adsorption or desorption currents. Thus the concentrations of copper and chloride in the reaction plane equal the bulk ones. In the absence of poisons the hydrogen current density reaches a diffusion limited plateau already for very small overpotentials (ca. 50 mV *vs.* RHE) reflecting that the HOR is one of the fastest known electrochemical reactions so that mass transport becomes the rate determining step. The measured and modeled maximum diffusion limited current densities, I_{diff}, agree within a factor of approximately 6, which is due to different transport conditions in model (large ring electrode) and experiment (small disk electrode). Additionally the experimental data obtained using a ring electrode with the dimensions given in Table 2 suggest that a smaller value of $k_H^a \approx 8 \times 10^{-3}\,\mathrm{cm\,s^{-1}}$ would match model and experiment.

Adding chloride yields a large region of negative differential resistance (NDR) following the steep current increase. The NDR gives rise to an autocatalytic loop composed of ϕ_{DL} and Cl^- (*cf.* Fig. 1), the general nature of which is well known and is described in various reviews [24–26]. Adding copper to the electrolyte solution inhibits H_2 oxidation almost completely at potentials negative to approximately 400 mV due to underpotential deposition of one monolayer of Cu. Starting from $\phi_{DL} \approx 400$ mV copper is stripped from the electrode and H_2 oxidation sets in until almost all copper left the surface and the current density corresponding to a copper-free solution is reached. Thus, the NDR due to Cl^- adsorption is hidden (turned into a positive differential resistance) in a certain potential interval. Hidden NDRs display oscillations if the process hiding the NDR, *i.e.* Cu^{2+} deposition, is much slower than the process that causes the NDR, *i.e.* Cl^- adsorption. Since the hidden NDR is part of an N-shaped i-ϕ_{DL} curve, these oscillators are commonly termed HN-NDR oscillators [26–28].

Calculating the dependence of the hydrogen current on the total coverage of the working electrode, the assumption made in Ref. [4] that, due to the fast transport, the hydrogen current density is only significantly reduced for total coverages above $\approx .8$ has to be dropped in favor of a standard langmuiric behavior.

Comparing the curves with Cu^{2+} and Cl^- in experiment and model it becomes apparent that the adsorption isotherm of Cu^{2+} underpotential deposition seems to be more positive than reported in [5]. Additionally the current decrease at higher potentials due to chloride adsorption is more pronounced in the model. A behavior closer to the model was observed in experiments using a ring working electrode. The ring electrode was not used for the comparison with the homogeneous model since spatial patterns can be expected which would lead to discrepancies especially in the time series of the oscillations (s.b.).

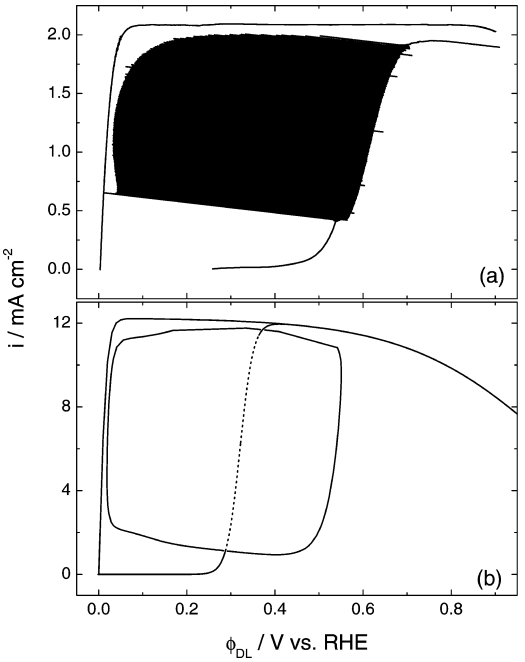

Fig. 3. (a) i as a function of ϕ_{DL} for an anodic potential scan in experiment. The scan rate is 2 mV s^{-1}, the concentrations were 1 mM Cl^-, 0.025 mM Cu^{2+} and 1 mM H_2SO_4; $R_t = 11\,k\Omega$. ϕ_{DL} was obtained from Eq. (5). (b) Oscillation amplitude and stationary states in the same plane calculated with the reduced four variable model using the parameters from Tables 1 and 2. Also shown are the curves without copper in the solution in both graphs to illustrate the importance of the potential dependence of the hydrogen current since the oscillations almost reach the Cu^{2+}-free curve.

3.2 Oscillatory behavior

For sufficiently high series resistance oscillations are observed in a wide range of applied voltages, U, on the branch of positive differential resistance in both, model and experiment. In Fig. 3(a) i is shown as a function of ϕ_{DL} for an anodic potential scan with a scan rate of 2 mV s^{-1}. For low applied voltages, U, the stationary low current state loses stability in a supercritical Hopf bifurcation. The amplitude of the oscillations increases very fast and soon extends from 400 mV to $\phi_{DL} \approx 0$. The same characteristics are obtained in the model as can be seen in Fig. 3(b), in which the oscillation amplitude obtained by a continuation of the model in the parameter U is depicted in the same plane. Observe that the oscillation amplitude almost reaches the current-voltage characteristic of the copper free system. It should be noted that the concentrations of Cl^- and Cu^{2+} used in the calculations were different from the ones used in the experiments. Especially the copper concentration had to be reduced by a factor of

approximately 20 to reproduce the diffusion limited adsorption as further discussed below. This could also be due to a slower adsorption rate constant $k_{\mathrm{Cu}}^{\mathrm{a},0}$ or a lower diffusion constant for our experimental situation which is reported in [29]. Another reason are the different transport conditions for a ring and a disk electrode (transport to a ring is more efficient than to a disk).

For the parameter values used in this paper oscillations do not exist for vanishing metal halide interaction strength χ illustrating the importance of the Cu^{2+}–Cl^{-} interaction. Note that in previous papers oscillations were also observed without taking the Cl^{-}–Cu^{2+} interaction into account using different and for our experimental situation unrealistic model parameters. The fast increase of the oscillation amplitude can only be captured for $\chi \gtrsim 10$ and was thus always absent in previous models. The drop of the double layer potential to $\phi_{\mathrm{DL}} \approx 0$ can only be modeled by taking c_{Cu} into account (*cf.* below). At current densities just below the maximum current density the oscillations vanish again in a Hopf bifurcation. The amplitude of the oscillations close to this second Hopf bifurcation again decreases fast, though not as fast as for lower potentials.

In Fig. 4 the time dependence of all seven variables is shown for a few oscillatory cycles. The almost exact similarity of the oscillatory form of ϕ_{DL} and $-i_{\mathrm{r}}$ seen in Fig. 4(a) stems from the fast double layer dynamics, *i.e.* capacitive currents remain small. The long active period of the current is caused by the slow diffusion limited adsorption of Cu^{2+} which can be seen in Fig. 4(b) and (c). While the copper concentration in the reaction plane is practically zero (dashed line in Fig. 4(b)), θ_{Cu} rises linearly until a threshold is reached and ϕ_{DL} increases fast. In the next section these findings will be used to simplify the model (6–12) considerably.

3.3 Model reduction

For the chloride concentrations used in experiments ($c_{\mathrm{Cl}} \geq 0.1$ mM) the chloride adsorption never becomes diffusion limited. Looking at Fig. 4 this becomes apparent through the absence of linear increases in chloride coverage, indicative of diffusion limited adsorption. It follows that the chloride concentration in the reaction plane remains almost constant (Fig. 4(b), solid line). In the following c_{Cl} is thus taken as constant $\left(c_{\mathrm{Cl}} \to c_{\mathrm{Cl}}^{\mathrm{b}}\right)$.

Regarding the variables governing the HOR, c_{H} and θ_{H}, it becomes apparent that the hydrogen coverage remains small during the whole cycle whereas c_{H} adjusts to a diffusion controlled value and stays approximately constant with changes below 2%. Rather than taking the hydrogen current density in the hydrogen saturated solution as a constant, as was done in [4] (see footnote 1), we conclude from these findings that the hydrogen current density can be modeled by

$$i_{\mathrm{H_2}} = (1 - \theta_{\mathrm{Cl}} - \theta_{\mathrm{Cu}})\, f(\phi_{\mathrm{DL}}) \tag{13}$$

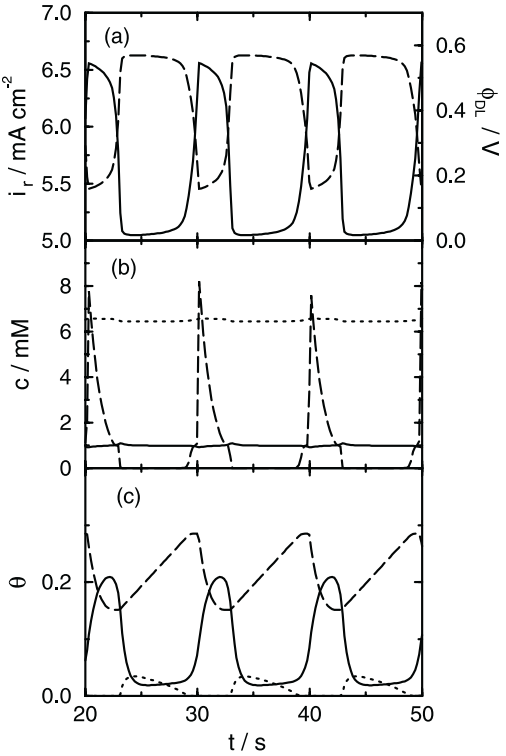

Fig. 4. Time evolution of i_r and the seven variables of model (6–12) for $U = 3$ V, other parameter values as in Tables 1 and 2. (a) ϕ_{DL} (solid line), i_r (dashed line). (b),(c) $1000\,c_{Cu}$, θ_{Cu} (dashed lines), $10\,c_{Cl}$, θ_{Cl} (solid lines) and c_H, θ_H (dotted lines).

with a function $f(\phi_{DL})$ fitted to simulated data using the above model or to the experimental data (*cf.* Fig. 2). This approach keeps in mind that low potentials are reached during the oscillations and thus the dependence of the hydrogen current density on the potential comes into play which was neglected in [4]. A suitable fit function is

$$f(\phi_{DL}) = c_1 \left(1 - 2(1 + e^{c_2 \phi_{DL}})^{-1}\right) .$$

In order to keep the model based on the known reaction steps, $f(\phi_{DL})$ was fitted to the theoretical hydrogen current density curve displayed in Fig. 2(b) (solid line) yielding $c_1 = 1.226 \times 10^{-2}$ A cm^{-2} and $c_2 = 118.7$ V^{-1}.

The reduced model thus consists of four equations, namely Eq. (6), which now reads

$$C\dot{\phi}_{DL} = -(1 - \theta_{Cl} - \theta_{Cu})c_1\left(1 - 2(1 + e^{c_2\phi_{DL}})^{-1}\right) + i\,, \qquad (14)$$

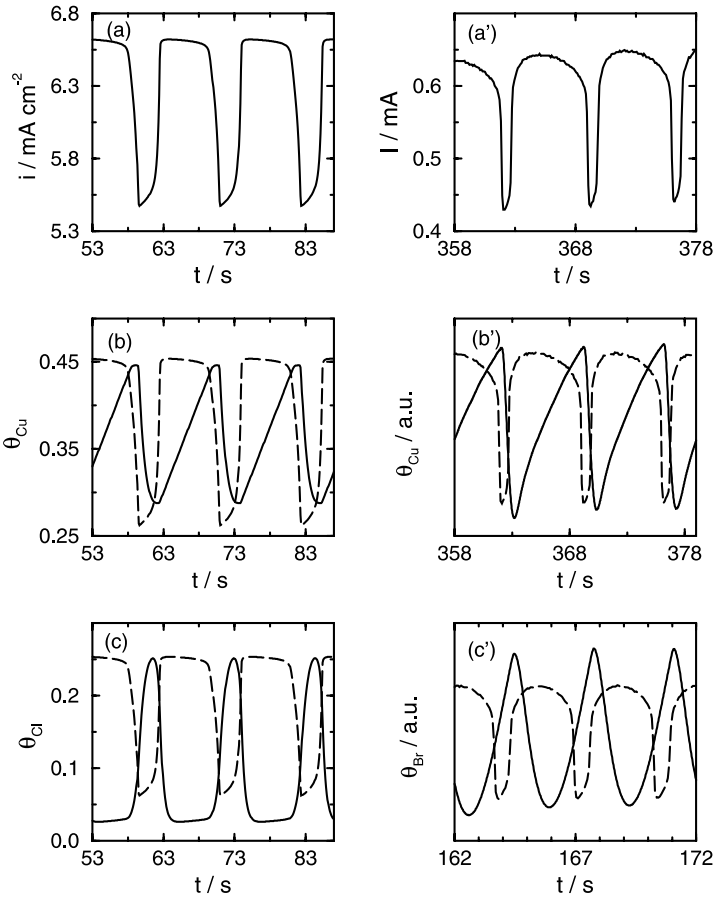

Fig. 5. (a)–(c) Oscillatory behavior of the four variable model to be compared with the full model, cf. Fig. 4, and with the experimental data (a')–(c'). The parameters used are given in Tables 1 and 2 and $U = 3$ V. (a')–(c') Experimental data obtained with the halide Br^- during an anodic potential scan with scan rate $5\,mV\,s^{-1}$ starting from 650 mV *vs.* SHE. Electrolyte: 0.5 M H_2SO_4, 0.01 mM $CuSO_4$, 0.01 mM HBr; $R_{ext} = 2.3\,k\Omega$. Further experimental details are given in the Appendix.

and Eqs. (8), (11), and (12) where c_{Cl} has to be substituted by c^b_{Cl} in the evolution equation for the chloride coverage, Eq. (12).

In Fig. 5(a)–(c) the time evolutions of ϕ_{DL}, θ_{Cu} and θ_{Cl} are shown as obtained with the above model. Comparing Fig. 5(a)–(c) to the data obtained with the full model eqns. (6–12), Fig. 4, it becomes apparent that, apart from a slight change in period, no deviation between the two models can be observed. The above four variable model is used in the next section for a detailed comparison with experiments.

3.4 Comparison of theory and experiment

In Fig. 5 theoretical and experimental data are compared. Shown are the total current density, the copper coverage and the halide coverage (using rate constants for Cl^- in the model but Br^- in experiment) for a few oscillatory cycles. The oscillation periods differ by about a factor of two, which is an exceptionally good agreement considering the use of 21 constants out of the literature, *i.e.* obtained by independent measurements,[3] and only one free parameter, the interaction strength χ. The agreement regarding the oscillatory form of all three quantities is apparent. The full descriptive power of the model, however, is displayed in the precise coincidence of the phase relations of calculated and experimental time series. In Fig. 5(b$^{(\prime)}$),(c$^{(\prime)}$) the current density is also plotted as a guide to the eye to compare the phase relations. Agreement exists concerning maxima and minima and slow and fast stages of the evolution of the coverages with respect to the evolution of ϕ_{DL}.

The precise agreement regarding the onset and amplitude of the oscillations was already demonstrated in Fig. 3 for a certain external resistance. In Fig. 6(a) the set of calculated Hopf bifurcation points in the R_t–U parameter plane in the model is compared with the points of onset of oscillations in experiment for 10 different values of the series resistance. This was done experimentally by varying the total resistance and measuring the voltage at which oscillations could first be observed, as illustrated in Fig. 6(b). It shows an experimental voltage scan for $R_t = 7\,\mathrm{k\Omega}$ (marked with the dotted line in Fig. 6(a)) and the points of onset of the oscillations in Fig. 6(b) correspond to the points on the dotted line in Fig. 6(a). The series resistance, R_t, in Fig. 6(a) is multiplied by the maximum diffusion limited reaction current, I_{diff}, observed in experiment and model respectively (*cf.* Fig. 2), to correct for different transport conditions. The remaining quantitative mismatch is due to the mismatch of the onset of Cu^{2+} desorption already discussed above (*cf.* Fig. 2).

4. Conclusions

The oscillatory mechanism during hydrogen oxidation on Pt is well understood. It is based on the opposite potential dependence of two poisons that adsorb at the working electrode and inhibit the hydrogen oxidation. This simple picture makes it an ideal model system since the dynamics can be controlled in model and experiment in a straight forward manner.

In earlier models these findings were used in a rough approximation that captured the basic oscillation mechanism [4–6]. Recent experiments reported in [12, 13] and experimental time series of i, ϕ_{DL}, θ_{Cu} and θ_{Br} presented in this paper showed that these earlier models failed to predict several features of the

[3] Note however that the six constants governing the chloride and copper adsorption velocities are poorly known (*cf.* Table 1) and that the copper concentration in the model is again lower as in experiment (s.a.).

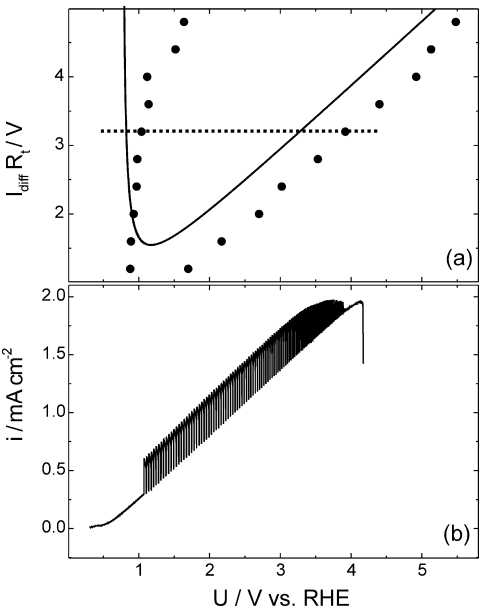

Fig. 6. (a) Oscillatory region in the $I_{\mathrm{diff}} R_{\mathrm{t}}$–$U$ plane. Solid line: Calculated Hopf bifurcations. Points: Experimentally observed locations of Hopf bifurcations for 10 different series resistances. The dotted line represents the scan displayed in (b). The error bars in the experiment are represented by the point size. The parameter values used in the experiment are the same as in Fig. 3(b). Example of an anodic voltage scan with a scan rate of $2\,\mathrm{mV\,s^{-1}}$ displaying the points of onset and ceasing of the oscillations and the oscillatory region for $R_{\mathrm{t}} = 7\,\mathrm{k\Omega}$.

experiments, including the amplitude, form, potential range and phase relations of the oscillations. But these features have to be captured by a model that is capable of describing the interesting spatio-temporal behavior observed in this system [12, 13].

In this paper we presented a detailed model of the oscillatory HOR in which all terms are well understood in their physical meaning. New experimental observations were included that describe an attractive interaction of chloride and copper on the electrode surface [1]. This proved to be essential even for the occurrence of oscillations for realistic model parameters.

We took into account the mass balance and transport equations for all three reacting species, H_2, Cl^- and Cu^{2+}, and the charge balance at the working electrode, thus arriving at a seven variable model. All constants that enter the seven evolution equations were taken from independent measurements out of the literature where possible. The unknown interaction strength between Cl^- and Cu^{2+} was adjusted to match model and experiments.

It was shown that the initial seven variable model could be reduced to a four variable one which is sufficient and minimal to give a quantitative description

of the presented experimental oscillations. Also the presented experimental bifurcation diagrams were shown to agree quantitatively with the ones calculated with the four variable model.

The thus solidly verified model can now be used in future studies of the rich spatio-temporal dynamics exhibited by this system in the presence of different spatial couplings [12, 13].

Acknowledgement

FP gratefully acknowledges financial support of the Deutsche Forschungsgemeinschaft in the framework of the Sonderforschungsbereich 555 "Complex Nonlinear Processes", project B4.

Appendix

Computational methods

The time integration was performed using lsode [30] with a relative tolerance of 10^{-15} and a time step of 10^{-4} s, which proved necessary due to the stiffness of the equations. The continuation package AUTO97 was used for the bifurcation diagrams [31].

Experimental methods

The experiments shown in Figs. 2, 3(a), and 6 were carried out with a polycrystalline Pt-disk of 5 mm in diameter, the one shown in Fig. 5(a')–(c') with ring-disk electrodes consisting of a polycrystalline Pt-disk ($\varnothing = 6$ mm) and either a Pt-ring or a Au-ring.

At the Pt-(Au-) ring changes in the coverage of Br^- (Cu^{2+}) on the Pt disk during the oscillations were probed. The ring-potential was set to 1380 mV *vs.* SHE to monitor changes in the bromide coverage (by measuring the Br_2 evolution current) and to 0 V *vs.* SHE to monitor changes in the copper coverage (through the Cu^{2+} deposition current). The coverages shown in Fig. 5(b') and (c') were obtained by integration of the ring currents.

The preparation of the electrodes and further experimental details are described in Ref. [4].

References

1. V. Stamenković and N. M. Marković, Langmuir **17** (2001) 2388.
2. M. Thalinger and M. Volmer, Z. Phys. Chem. **150** (1930) 401.
3. G. Horányi and C. Visy, J. Electroanal. Chem. **103** (1979) 353.
4. K. Krischer, M. Lübke, W. Wolf, M. Eiswirth, and G. Ertl, Electrochim. Acta **40** (1995) 69.
5. W. Wolf, K. Krischer, M. Lübke, M. Eiswirth, and G. Ertl, J. Electroanal. Chem. **385** (1995) 85.

6. W. Wolf, M. Lübke, M. T. M. Koper, K. Krischer, M. Eiswirth, and G. Ertl, J. Electroanal. Chem. **399** (1995) 185.
7. G. Horányi and G. Vértes, J. Electroanal. Chem. **45** (1973) 295.
8. K. Krischer, M. Lübke, W. Wolf, M. Eiswirth, and G. Ertl, Ber. Bunsenges. Phys. Chem. **95** (1991) 820.
9. M. Eiswirth, M. Lübke, K. Krischer, W. Wolf, J. L. Hudson, and G. Ertl, Chem. Phys. Lett. **192** (1992) 254.
10. K. Krischer, M. Lübke, M. Eiswirth, W. Wolf, J. L. Hudson, and G. Ertl, Physica D **62** (1993) 123.
11. W. Wolf, Ph. D. Thesis, Freie Universität Berlin, Berlin, Germany (1994).
12. H. Varela and K. Krischer, Catal. Today **70** (2001) 411.
13. P. Grauel, H. Varela, and K. Krischer, Faraday Disc. **120** (2001) 165.
14. N. Marković and P. N. Ross, Langmuir **9** (1993) 580.
15. N. M. Marković, B. N. Grgur, and P. N. Ross, J. Phys. Chem. B **101** (1997) 5405.
16. C. H. Hamann, A. Hamnett, and W. Vielstich, Electrochemistry, Wiley/VCH, Weinheim (1998).
17. Y. Mukouyama, S. Nakanishi, T. Chiba, K. Murakoshi, and Y. Nakato, J. Phys. Chem. B **105** (2001) 7246.
18. J. Barber, S. Morin, and B. E. Conway, J. Electroanal. Chem. **446** (1998) 125.
19. R. Mills and V. M. M. Lobo, *Self-Diffusion in Electrolyte Solutions*, Elsevier, New York (1989), p. 320.
20. G. Horányi, Electrochim. Acta **25** (1980) 43.
21. N. M. Marković, H. A. Gasteiger, and P. N. Ross, Langmuir **11** (1995) 4098.
22. N. M. Marković, H. A. Gasteiger, C. A. Lucas, I. M. Tidswell, and P. N. Ross, Surf. Sci. **335** (1995) 91.
23. S. Nakanishi, Y. Mukouyama, K. Karasumi, A. Imanishi, N. Furuya, and Y. Nakato, J. Phys. Chem. B **104** (2000) 4181.
24. M. T. M. Koper, in *Advances in Chemical Physics* (eds. I. Prigogine and S. A. Rice), Vol. 92, Wiley, New York (1996), p. 161.
25. K. Krischer, in *Modern Aspects of Electrochemistry* (eds. B. E. Conway, J. O. Bockris, and R. White), Vol. 32, Kluwer Academic/Plenum Publishers, New York (1999) p. 1.
26. K. Krischer, J. Electroanal. Chem. **501** (2001) 1.
27. M. T. M. Koper, J. Electroanal. Chem. **409** (1996) 175.
28. K. Krischer, N. Mazouz, and P. Grauel, Angew. Chem.–Int. Ed. **40** (2001) 851.
29. J. Newman, *Electrochemical systems*, Prentice Hall, Englewood Cliffs, second edn. (1991).
30. A. C. Hindmarsh, ACM-SIGNUM Newsl. **15** (1980). lsode is available from the netlib library http://www.netlib.org/odepack/.
31. E. J. Doedel and J. P. Kevernez, *Auto: Software for continuation and bifurcation problems in ordinary differential equations*, Applied mathematics report, California Institut of Technology (1986).
    AUTO is available from http://indy.cs.concordia.ca/auto/.